HHS Public Access

Author manuscript

*Hear Res*. Author manuscript; available in PMC 2020 January 11.

Published in final edited form as:

*Hear Res*. 2018 July ; 364: 48–58. doi:10.1016/j.heares.2018.04.001.

# Functions of CaBP1 and CaBP2 in the peripheral auditory system

**Tian Yang**[a,b], **Ning Hu**[b,c], **Tina Pangrsic**[d], **Steven Green**[b,c], **Marlan Hansen**[b,e], **Amy Lee**[a,b,f]

[a]Department of Molecular Physiology and Biophysics, University of Iowa, Iowa City, IA 52242, USA

[b]Department of Otolaryngology Head-Neck Surgery, University of Iowa, Iowa City, IA 52242, USA

[c]Department of Biology, University of Iowa, Iowa City, IA 52242, USA

[d]Synaptic Physiology of Mammalian Vestibular Hair Cells Group, Institute for Auditory Neuroscience and InnerEarLab, University Medical Center Göttingen, Göttingen, Germany

[e]Department of Neurosurgery, University of Iowa, Iowa City, IA 52242, USA

[f]Department of Neurology, University of Iowa, Iowa City, IA 52242, USA

## Abstract

CaBPs are a family of $Ca^{2+}$ binding proteins related to calmodulin. Two CaBP family members, CaBP1 and CaBP2, are highly expressed in the cochlea. Here, we investigated the significance of CaBP1 and CaBP2 for hearing in mice lacking expression of these proteins (CaBP1 KO and CaBP2 KO) using auditory brain responses (ABRs) and distortion product otoacoustic emissions (DPOAEs). In CaBP1 KO mice, ABR wave I was larger in amplitude, and shorter in latency and faster in decay, suggestive of enhanced synchrony of auditory nerve fibers. This interpretation was supported by the greater excitability of CaBP1 KO than WT neurons in whole-cell patch clamp recordings of spiral ganglion neurons in culture, and normal presynaptic function of CaBP1 KO IHCs. DPOAEs and ABR thresholds were normal in 4-week old CaBP1 KO mice, but elevated ABR thresholds became evident at 32 kHz at 9 weeks, and at 8 and 16 kHz by 6 months of age. In contrast, CaBP2 KO mice exhibited significant ABR threshold elevations at 4 weeks of age that became more severe in the mid-frequency range by 9 weeks. Though normal at 4 weeks, DPOAEs in CaBP2 KO mice were significantly reduced in the mid-frequency range by 9 weeks. Our results reveal requirements for CaBP1 and CaBP2 in the peripheral auditory system and highlight the diverse modes by which CaBPs influence sensory processing.

### Keywords

spiral ganglion; hair cells; $Ca^{2+}$ channels; $Ca^{2+}$ sensor

Corresponding author: Amy Lee, Dept. of Molecular Physiology and Biophysics, University of Iowa, PBDB 5318, 169 Newton Road, Iowa City, IA 52242, Phone: (319) 384-1762, Fax: (319) 335-7330 amy-lee@uiowa.edu.

## 1. Introduction

Elevations in intracellular $Ca^{2+}$ regulate a vast array of cellular processes including gene transcription, cell migration, and the synaptic release of neurotransmitters. How $Ca^{2+}$ signals are decoded and specifically coupled to downstream signaling pathways is a fundamental question in cell biology. The ubiquitous $Ca^{2+}$ sensor calmodulin (CaM) is the primordial member of a superfamily of EF-hand $Ca^{2+}$ binding proteins and a key mediator of $Ca^{2+}$-dependent processes. There are 4 EF-hand $Ca^{2+}$ binding motifs in CaM that upon binding $Ca^{2+}$ trigger conformational changes that allow CaM to interact with and regulate effectors such as ion channels, enzymes, and transcription factors (Chin et al., 2000).

Yet, CaM is but one of many $Ca^{2+}$ sensors in the nervous system. Multiple CaBP family members are expressed in the cochlea (Cui et al., 2007; Yang et al., 2006) of which CaBP1 and CaBP2 are the most abundant (Yang et al., 2016). In heterologous expression systems, CaBP1 and CaBP2 strongly potentiate the function of voltage-gated $Ca_v1.3$ $Ca^{2+}$ channels by suppressing voltage- and/or $Ca^{2+}$-dependent inactivation (Cui et al., 2007; Picher et al., 2017; Yang et al., 2006). This effect of CaBPs may be physiologically relevant since $Ca_v1.3$ channels mediate the release of glutamate at the inner hair cell (IHC) synapse and show much less $Ca^{2+}$-dependent inactivation in IHCs than in recombinant systems (Koschak et al., 2001; Platzer et al., 2000). CaBP2 is highly expressed in IHCs (Picher et al., 2017; Yang et al., 2016), and mutations in the gene encoding CaBP2 cause autosomal recessive hearing loss in humans (Picher et al., 2017; Schrauwen et al., 2012). Within the cochlea, CaBP1 is most highly expressed in spiral ganglion neurons (SGNs) and possibly satellite glial cells, which do not express CaBP2 (Yang et al., 2016). Based on their differences in expression within the cochlea, we hypothesized that CaBP1 and CaBP2 may have distinct roles in peripheral auditory function.

To test this, we analyzed the function of SGNs and ascending auditory pathways of mice lacking expression of CaBP1 or CaBP2 by measuring auditory brainstem responses (ABRs) and assessed the function of outer hair cells (OHCs) by measuring distortion product otoacoustic emissions (DPOAEs). In addition, we performed electrophysiological recordings of SGNs and cochlear IHCs to probe the cellular mechanism underlying the auditory phenotype of CaBP1 KO mice.

## 2. Materials and methods

### 2.1 Animals

All experiments were performed in accordance with guidelines set by the Office of the Institutional Animal Care and Use Committee at the University of Iowa and University Medical Center Göttingen. The procedures used in this study are not expected to produce pain or suffering in the animals. Generation of CaBP1 KO mice (RRID: MGI: 5780462) and CaBP2 KO mice was described previously (Kim et al., 2014; Sinha et al., 2016). Mice were maintained on a C57BL/6N (for CaBP1 KO) or C57BL/6J (for CaBP2 KO) background strains and housed in groups on a standard 12:12 hour light: dark cycle, with food and water provided ad libitum. Mice from post-natal days (P) 16–23, 4-week, 9-week and 6-month of mixed sexes were used in this study.

### 2.2. ABRs and DPOAEs

Mice were anesthetized with an intraperitoneal injection of ketamine/xylazine/Acetopromazine (100, 15 and 5 mg/kg body weight, respectively) before all experiments. Body temperature was maintained with a heating pad. All recordings were completed in a custom-made soundproof acoustic chamber using a Tucker-Davis (TDT) BioSig System III (Tucker-Davis Technologies, Alachua, FL).

The ABR in response to tone-pips with duration of 5 ms and gated time of 0.5 ms, presented at rate of 21/s and at frequencies of 8, 16, 32kHz, alternative polarities, was recorded with subcutaneous platinum needle electrodes placed at the vertex (non-inverting input), behind the ear being recorded (inverting input), and a ground electrode at the low back area. Stimulus sound was delivered to the external auditory meatus of a mouse through a custom-made insertion tube connected to the MF1 speaker. The acquisition time was 12 ms at sampling rate of 25,000/s with a band-pass filter between 300 to 3000 Hz. The signals are averaged by 128–1024 sweeps. The threshold was determined as the lowest stimulus intensity (dB SPL) which produced 2 – 3 replicable ABR waveforms. Wave I amplitude was defined as $I_n$-$I_p$ (latency 1 – 2.2 ms). Quantitative analysis of ABR amplitudes was determined by custom-written routines in Excel (Microsoft).

DPOAE stimuli were digitally synthesized using SigGen software applications. Stimulation of two primary tones f1 and f2 (frequency f2/f1 = 1.2) was presented at the same intensity ranging from 40 to 80 dB SPL in 10 dB SPL increments. The stimuli were calibrated in a 0.1-mL coupler simulating the mouse ear canal. Sound pressure was recorded with an ER10B+ Low Noise microphone and probe (Etymotic) housed in the same coupler as the f1 and f2 speakers. DPOAE amplitudes at 2f1- f2 were measured automatically with SigGen. Noise floor was determined as the baseline amplitude around the 2f1- f2 (average amplitude of the first five points before and first five points after 2f1- f2). Since there was significant decrease in noise floor in CaBP2 KO mice compared with WT mice, the difference between the DPOAE amplitude and the noise floor was plotted for each genotype.

### 2.3. Electrophysiology

Dissociated SGN cultures were prepared according to a previously described protocol (Lv et al., 2012) with modification. Briefly, cochlear tissue was dissected from P16–23 mice in $Ca^{2+}$/$Mg^{2+}$-free Hank's Balanced Salt Solution (HBSS) and digested in an enzyme mixture containing collagenase type I (1 mg/mL, ThermoFisher 17100) and DNase I (1 mg/mL, Sigma DN25) at 37°C for 25 min. After gentle triturations, the cells were plated on poly-L-ornithine/laminin-coated coverslips in Nunclon 4-Well PS MultiDish (Thermo Scientific). SGNs were maintained in Neurobasal-A culture media supplemented with 2% B27 (v/v), 2 mM L-glutamine, 1x penicillin-Streptomycin, 25 ng/mL BDNF (Sigma B3795) and 25 ng/mL NT3 (Sigma N1905). All media and supplement were from Gibco™ unless noted otherwise.

About 24–72 h after plating SGNs, whole-cell patch clamp recordings were performed at room temperature. Electrodes (2–4 MΩ) were pulled from borosilicate glass and were filled with solution containing the following (in mM): 150 KCl, 10 HEPES, 10 D-glucose, pH 7.3.

The external solution contained (in mM): 145 NaCl, 6 KCl, 1 $MgCl_2$, 2 $CaCl_2$, 10 D-glucose, and 10 HEPES, pH 7.3. The series resistance was monitored during the course of the experiments and the liquid junction potential (- 3mV) were measured and corrected. As described previously (Lv et al., 2012; Lv et al., 2014), a stable giga-ohm seal was established for at least 5 min before data collection.

For patch-clamp recordings of IHCs, CaBP1 KO and WT control mice (P17–22) were used. The apical cochlear turns were dissected in HEPES Hank's solution containing (in mM): 5.36 KCl, 141.7 NaCl, 1 $MgCl_2$, 0.5 $MgSO_4$, 10 HEPES, 11.1 D-glucose and 3.42 L-glutamine, pH: 7.2. IHCs from the middle/basal part of the apical turn were patch-clamped in the perforated-patch configuration. The pipette solutions contained (in mM): 130 Cs-gluconate, 10 TEA-Cl, 10 4-AP (4-aminopyridine; Merck KGaA), 1 $MgCl_2$, 10 HEPES, 300 μg/ml amphotericin B (Merck KGaA), pH 7.17, ~290 mOsm. The extracellular solutions contained (in mM): 111 NaCl, 35 TEA-Cl, 2.8 KCl, 2 $CaCl_2$, 1 $MgCl_2$, 10 HEPES, 1 CsCl, 0.1 apamin (PeptaNova GmbH, Sandhausen, Germany), 11.1 D-glucose, pH 7.2, ~300 mOsm. All chemicals were obtained from Sigma-Aldrich unless stated otherwise. Recordings were done at room temperature with an EPC-9 amplifier controlled by Pulse software (HEKA).

To measure $Ca^{2+}$ current inactivation in IHCs, 500-ms depolarizations to −14 mV were used. Membrane capacitance changes ($\Delta C_m$) were measured as previously described (Moser and Beutner, 2000). Data were averaged 400 ms before and after depolarization, skipping the first 100 ms after depolarization. Depolarizations (2–100 ms duration) consisted of voltages evoking peak $Ca^{2+}$ current amplitudes at intervals of 30 to 120 s as well as trains of depolarizations (20 10-ms long depolarizations at 1/114 $ms^{-1}$). All voltages were corrected for liquid junction potential (−14 mV) and data were analyzed with Igor Pro (Wavemetrics Inc.) software. For statistical analysis, data were tested for randomness, normality (Jarque-Bera test), and equality of variances (F-test), and compared for statistical significance using Student's t test or Wilcoxon's rank-sum test, as appropriate.

### 2.4. Quantitation of inner hair cell synapses

Mice (9-week-old) were anesthetized with isoflurane and decapitated. Inner ears were quickly removed from the skull to ice-cold PBS. Round and oval windows were opened, and the bone over the apex of the cochleae was removed. Cochleae were fixed in 4% PFA in PBS for 10 min with gentle agitation. After de-calcification in 10% EDTA in PBS for 24 h, the cochleae were dissected and processed for immunofluorescence. The tissue was blocked for 1 h with blocking buffer, and incubated with primary antibodies diluted in blocking buffer for 24 – 36 h at 4 °C (CtBP2, 1:200, BD Biosciences Cat# 612044 RRID:AB_399431; GluR2/3, 1:200, Abcam Cat# ab52896 RRID:AB_880229). After washing in PBS, the tissue was incubated with secondary antibodies Alexa 488 (1:500, Cat# A-11017, RRID:AB_2534084) and Alexa 568 (1:500; Cat# A21069, RRID:AB_10563601, both from Thermo Fisher Scientific) for 1 hour at room temperature. After washing 3 times with PBS, the cochleae were mounted in glycerol and imaged with a confocal laser scanning microscope (Olympus Fluoview 1000) using a 60X oil-immersion objective and FluoView software (RRID: SCR_014215). In confocal z-stacks of images, the number of synapses per

inner hair cells was determined as the number of structures with juxtaposed CtBP2- and GluR2/3- labeling divided by the total number of inner hair cell nuclei which were also labeled by CtBP2 antibodies. Assignment of synapse counts to cochlear regions corresponding to tonotopic frequencies (8, 16, and 32 kHz) was estimated according to position along the length of the cochlea based on data from Meyer et al (Meyer et al., 2009).

### 2.5. Experimental design and statistical analysis

For all the experiments, males and females were used. Whenever possible, WT and CaBP1 KO samples were prepared and analyzed in parallel. Statistical analysis was done with Graphpad Prism software 7 (RRID: SCR_002798). An alpha level of 0.05 was used for all statistical tests. Data were first tested by Shapiro-Wilk normality test. If the data were normally distributed, unpaired *t* test or ANOVA with post hoc Bonferroni's multiple comparisons test was performed. Otherwise, Kolmogorov-Smirnov test, Brown–Forsythe test, or polynomial curve fitting was performed. For 2-way ANOVA, the main effects were reported if there was no significant interaction, and post hoc analysis was performed on the main effects that had more than two levels. Otherwise, post hoc tests were performed and simple main effects were reported using adjusted *p* value for multiple comparisons. Brown-Forsythe test was performed with R (R Project for Statistical Computing). Three significant digits for *p* values were reported. Error bars represented standard deviation (SD) for scatter plots, and standard error of the mean (SEM) for the rest of the graphs.

## 3.0 Results

### 3.1. DPOAEs are not altered but ABR thresholds are elevated in CaBP1 KO mice

Alternative splicing results in 3 CaBP1 variants (CaBP1-S, CaBP1-L, and caldendrin), of which caldendrin is most abundant in the cochlea (Yang et al., 2016). To investigate the auditory function of CaBP1, we used mice that lack expression of all 3 CaBP1 splice variants (Kim et al., 2014). Based on the expression of CaBP1 in IHCs and OHCs (Yang et al., 2016), we expected that ABR thresholds might be impacted in CaBP1 KO mice. To isolate the effect of CaBP1 knockdown on OHCs, we analyzed DPOAEs in which the function of OHCs in the electromechanical amplification of sound can be assessed. In mice at age 4 weeks, 9 weeks, and 6 months, DPOAEs were measured in response to stimuli consisting of two primary tones of distinct frequency (f1 and f2, f2/f1 = 1.2). DPOAE amplitudes were measurable above the noise floor and across frequencies, and not significantly different between WT and CaBP1 KO mice at all ages tested (Fig. 1). We next compared ABRs in WT and CaBP1 KO mice using stimuli consisting of brief tone pips of different frequencies and intensities. Comparisons of representative ABRs from WT and CaBP1 KO mice are shown in Fig. 2A–C. While ABR thresholds were generally not affected in younger CaBP1 KO mice (Fig. 1A,B), they were slightly elevated above WT levels by 6 months of age (Fig. 2C). Thus, OHC function is not affected in CaBP1 KO mice.

### 3.2. Auditory nerve responses are augmented in CaBP1 KO mice

Within the cochlea CaBP1 is most abundant in the spiral ganglion (Yang et al., 2016), which contains the cell bodies of SGNs that transmit acoustic information from IHCs to the brainstem via the auditory nerve. Based on this localization, we expected that CaBP1 KO

mice might have defects in evoked auditory nerve activity. To test this, we scrutinized ABRs of CaBP1 KO mice for alterations in wave I, which represents the summed activity of auditory nerve axons in response to auditory stimulation. In 9 week-old CaBP1 KO mice, wave I was greater in amplitude and shorter in latency when using 8 kHz and 16 kHz tone pips compared to WT mice (Fig. 3A,B). The interval between the positive (P1) and negative (N1) components of wave I, which represents the decay of the population SGN response (Hall, 2007), was significantly shorter in CaBP1 KO than WT mice (Fig. 3C). This result implies greater synchrony among auditory nerve fibers, which can account for the increased wave I amplitudes in CaBP1 KO mice.

### 3.3. The number of IHC synapses is normal in CaBP1 KO mice

The alterations in wave I of CaBP1 KO ABRs could also result from increased IHC synaptic transmission from IHCs to SGN afferents, due to more numerous IHC synapses in the cochlea of CaBP1 KO mice. To investigate this possibility, we counted IHCs synapses in the cochleae of 9-week old WT and CaBP1 KO mice that were double-labeled with antibodies against CtBP2 and GluR2/3 to delineate the presynaptic and postsynaptic, respectively, sides of the IHC synapse. The tonotopic position of synapses was estimated according to position along the length of the cochlea (Meyer et al., 2009). By this method, the number of IHC synapses was not significantly different in CaBP1 KO and WT mice in the cochlear locations corresponding to the ABR test frequencies (Fig. 4; $F(1,34) = 0.6734$, $p = 0.4176$ by two-way ANOVA).

### 3.4. $Ca^{2+}$ channel function and exocytosis is normal in CaBP1 KO IHCs

The wave I abnormalities in CaBP1 KO ABRs could also be due to changes in presynaptic $Ca^{2+}$ influx in IHCs that would lead to enhanced $Ca^{2+}$-triggered exocytosis of glutamate at the active zones of IHCs. To test this, we performed perforated-patch clamp recordings of IHCs to measure whole cell $Ca^{2+}$ currents ($I_{Ca}$) and changes in membrane capacitance ($\Delta C_m$) reflecting exocytosis of synaptic vesicles. In these experiments, $I_{Ca}$ amplitudes and voltage-dependence of activation were comparable in IHCs of the CaBP1 KO and age-matched control mice upon short depolarizations to different potentials (Fig. 5A). Inactivation of $I_{Ca}$ during 500-ms long step depolarizations to −14 mV was also not affected in CaBP1 KO IHCs (Fig. 5B). Finally, there were no significant differences in $\Delta C_m$ evoked by single 2–100-ms long (Fig. 5D) or repetitive short depolarizations (Fig. 5E) in control and CaBP1 KO IHCs. Taken together, these results suggest that the observed changes in wave I in ABRs of CaBP1 KO mice are most likely due to effects downstream of the IHC ribbon synapse.

### 3.5. Input resistance is decreased in CaBP1 KO SGNs

To test if the alterations in auditory nerve activity could result from heightened excitability of C-KO SGNs, we performed whole-cell current clamp recordings of SGNs in cultures prepared from hearing mice (P16–23). We analyzed separately SGNs that were rapidly adapting (Fig. 6A–D) and slowly adapting (Fig. 6E–H) based on previously described criteria (Lv et al., 2012). In these experiments, there was no difference in resting membrane potential or action potential (AP) threshold, latency, or amplitude between WT and CaBP1 KO SGNs (Table 1). However, there was less variance in the half-width of the threshold-

evoked AP in rapidly and slowly adapting neurons from CaBP1 KO than from WT mice (Fig. 6C,G). When the data from slowly adapting and fast- adapting neurons were combined, there was a trend towards shorter AP half-widths in CaBP1 KO than in WT SGNs although this did not reach statistical significance (Kolmogorov-Smirnov $D = 0.347$, $p = 0.093$). The input resistance, estimated from the slope of the linear fit of the current versus steady-state voltage relationship, was slightly but significantly smaller in CaBP1 KO SGNs (Fig. 6D,H). Reducing the input resistance should decrease the response latency and speed AP kinetics, and therefore could contribute to the more consistent AP durations and the distinctions in CaBP1 KO ABRs: shorter ABR wave I latency and more synchronized firing of auditory nerve fibers.

### 3.6. ABRs indicate progressive hearing loss in CaBP2 KO mice

We next analyzed ABRs and DPOAEs of CaBP2 KO mice. These mice were generated by replacing exons 1 and 2A with tdTomato and PGK neo cassette as well as stop codons in all 3 reading frames of exon 2B, which should prevent expression of all CaBP2 splice variants (Sinha et al., 2016). In contrast to the normal ABRs of 4 week-old CaBP1 KO mice (Fig. 2A), ABR thresholds at 8 and 32 kHz were elevated in CaBP2 KO mice at this age (Fig. 7A). By 9 weeks of age, ABR threshold elevations became significant in the mid-frequency range of CaBP2 KO mice (Fig. 7B). Thus, CaBP2 KO mice exhibit hearing loss that is more severe and earlier in onset as compared to CaBP1 KO mice.

### 3.7. DPOAEs indicate age-related impairment in OHC function

In contrast to CaBP1 KO mice (Fig. 1), DPOAEs were significantly affected in CaBP2 KO mice. Although normal at 4 weeks of age, DPOAE amplitudes were significantly reduced in 9-week old CaBP2 KO mice particularly in the mid-frequency range and in response to high-intensity stimuli (Fig. 8). These results suggest that unlike in CaBP1 KO mice, the function of the OHCs and/or cochlear amplifier is impaired in CaBP2 KO mice.

## 4.0 Discussion

### 4.1. Role of CaBP1 in hair cells

The complex auditory phenotype of CaBP1 KO mice is consistent with the expression of CaBP1 in multiple cochlear cell-types (Yang et al., 2016). By in situ hybridization, we previously found that the shorter CaBP1 splice variants (CaBP1-S and/or CaBP1-L) were expressed in both IHCs and OHCs (Yang et al., 2016). DPOAEs, which reflect the function of OHCs, were normal in CaBP1 KO mice (Fig. 1). Thus, the elevated ABR thresholds in older CaBP1 KO mice may result from defects in IHCs and/or in SGNs rather than OHCs. How CaBP1 might contribute to the function of IHCs is unclear. In transfected cells, CaBP1 strongly suppresses $Ca^{2+}$-dependent inactivation of $Ca_v1.3$ channels (Cui et al., 2007), which are the major presynaptic $Ca^{2+}$ channels regulating exocytosis in IHCs (Brandt et al., 2003; Platzer et al., 2000). Thus, loss of CaBP1 would be expected to increase $I_{Ca}$ inactivation, and possibly decrease evoked exocytosis, in IHCs. However, patch clamp recordings of CaBP1 KO IHCs revealed no changes in the properties of the whole-cell $I_{Ca}$ or exocytosis (Fig. 5). While this result might stem from the compensatory effects of other CaBPs such as CaBP2 (Cui et al., 2007; Picher et al., 2017; Schrauwen et al., 2012), the

importance of CaBP1 in regulating IHC function may depend on its interactions with targets other than $Ca_V1.3$ . These include calmodulin-dependent protein kinase II (Haeseleer et al., 2000) and AKAP79/150 (Gorny et al., 2012). In addition, CaBP1 inhibits inositol trisphosphate receptors (Haynes et al., 2004; Kasri et al., 2004), which are highly expressed in IHCs (Liu et al., 2015). Understanding the role of CaBP1 in IHCs is an important challenge for future studies.

### 4.2. Role of CaBP1 in the spiral ganglion

The increased amplitudes and shorter latencies of wave I in CaBP1 KO ABRs can be explained by the decreased input resistance (Fig. 6D,H) and subsequent shortening of the membrane time constant in CaBP1 KO SGNs. Moreover, decreased latency in the population of auditory nerve fibers could result in greater synchrony among them and hence increased wave I amplitude. This possibility is supported by the observed decreased P1-N1 interval (Fig. 3C). A possible cause of the decreased input resistance in CaBP1 KO SGNs could be enhanced opening of voltage-gated $K^+$ channels (Mo et al., 2002).

In addition to its effects on $Ca_V1$ channels, CaBP1 strongly inhibits $Ca_V2.1$ (P/Q-type) channels (Lee et al., 2002) that are also expressed in SGNs (Chen et al., 2011). Since blockade of $Ca_V2.1$ channels decreases the amplitude and increases the latency of SGN APs (Lv et al., 2012), enhanced function of $Ca_V2.1$ channels in CaBP1 KO SGNs would be expected to facilitate SGN firing and therefore could also contribute to the alterations in wave I in CaBP1 KO ABRs (Fig. 3).

### 4.3. CaBP2 is required for hair cell function

Unlike CaBP1, CaBP2 is not expressed in the brain (Haeseleer et al., 2000). Moreover in the cochlea, CaBP2 is only detected at the mRNA level in hair cells (Yang et al., 2016). In neonatal (~P7) mice, CaBP2 expression is restricted to IHCs, with comparatively weaker expression in OHCs becoming evident in older mice (Picher et al., 2017; Yang et al., 2016). Based on this expression pattern, CaBP2 may regulate $Ca^{2+}$ signaling pathways necessary for the function of IHCs since ABR threshold elevations were already evident in 4-week old CaBP2 KO mice without alterations in DPOAEs (Figs. 7A, 8A). The later onset of CaBP2 expression in OHCs may explain why the function of OHCs is compromised at a later stage (9 weeks; Fig. 8B) than IHCs in CaBP2 KO mice.

Our results are in general agreement with previous analyses of a distinct CaBP2 null line ($CaBP2^{LacZ/LacZ}$; (Picher et al., 2017)) with some differences. While we found ABR thresholds to be elevated in the low- and high-frequency range in our CaBP2 KO mice at 4 weeks of age (Fig. 7A), $CaBP2^{LacZ/LacZ}$ mice show significant threshold elevations in the mid-frequency range at this age (Picher et al., 2017). Moreover, $CaBP2^{LacZ/LacZ}$ mice did not show any alterations in DPOAEs (Picher et al., 2017), in contrast to the compromised DPOAEs in our CaBP2 KO mice at 9 weeks of age (Fig. 8B). Possible explanations for these discrepancies involve differences in gene targeting strategies and background mouse strains. In this context, it is noteworthy that human mutations cause variable OHC phenotypes as measured in transient evoked otoacoustic emissions (TEOAs) (Picher et al., 2017;

Schrauwen et al., 2012)). Thus, loss-of function of CaBP2 may differentially impact OHC function depending on genetic modifiers, and/or other influences.

The auditory phenotype of our CaBP2 KO mice is consistent with that of humans bearing a splice-site mutation in CaBP2 causing sensorineural hearing loss. Affected individuals exhibit hearing loss that is most severe in the mid-frequency range and a lack of TEOAEs (Schrauwen et al., 2012) suggestive of OHC dysfunction. Although a role for CaBP2 in suppressing voltage-dependent inactivation of $Ca_V1.3$ channels in IHCs of $CaBP2^{LacZ/LacZ}$ mice has been demonstrated (Picher et al., 2017), the function of CaBP2 in OHCs remains to be elucidated. $Ca_V1.3$ channels are also expressed in OHCs (Michna et al., 2003), where they may regulate exocytosis that can activate type II afferent neurons (Weisz et al., 2012). Based on the modulation of $Ca_V1.3$ by CaBP2 in transfected cells (Schrauwen et al., 2012), CaBP2 may prolong $I_{Ca}$ in OHCs which may maximize rates of OHC exocytosis and strengthen synaptic transfer to type II afferents. Alternatively, CaBP2 may regulate $Ca^{2+}$ signaling pathways that influence the electromotile and sound-amplifying properties of OHCs (Dulon et al., 1991) as has been proposed for the $Ca^{2+}$ binding protein oncomodulin which is also necessary for OHC function (Tong et al., 2016).

A technical consideration is that our CaBP KO mouse lines were bred on different genetic backgrounds: C57BL/6N (for CaBP1 KO) or C57BL/6J (for CaBP2 KO). These background strains show differences in auditory function (Kendall et al., 2014) (but see (Simon et al., 2013)), so it is possible that the genetic background may influence the impact of CaBP knockdown. For this reason, we have avoided direct comparisons of the roles of CaBP1 and CaBP2 in the inner ear based in our study.

## 5.0 Conclusions

In this study, we demonstrate that CaBP1 and CaBP2 are required for the normal function of the peripheral auditory system. Loss of CaBP1 modestly increases ABR thresholds only in older mice but has a profound effect in enhancing auditory nerve synchrony, as indicated by the increased amplitude, shorter latency, and decreased width of wave I in ABRs of CaBP1 KO mice. Loss of CaBP2 causes significant ABR threshold elevations and depressed DPOAE amplitudes that become more severe with age in the mid-frequency range. Our findings advance our understanding of the physiological functions of CaBP family members, and provide insight into how dysregulation of such $Ca^{2+}$ sensors can lead to hearing impairment.

## Acknowledgements

This work was supported by grants from the NIH (NS084190, DC009433 to A.L.; DC010362 (Iowa Center for Molecular Auditory Neuroscience); U.S. Department of Defense (MR130438 to S.H.G, M. H and A.L); the German Research Foundation (DFG Priority Program 1608, PA 2769/1–1, to T.P.); and the Roy J. Carver Charitable Trust to A.L.

## References

Brandt A, Striessnig J, Moser T 2003 CaV1.3 channels are essential for development and presynaptic activity of cochlear inner hair cells. J. Neurosci. 23, 10832–10840.

Chen WC, Xue HZ, Hsu YL, Liu Q, Patel S, Davis RL 2011 Complex distribution patterns of voltage-gated calcium channel alpha-subunits in the spiral ganglion. Hear Res 278, 52–68. [PubMed: 21281707]

Chin D, Means AR 2000 Calmodulin: a prototypical calcium sensor. Trends Cell Biol 10, 322–328. [PubMed: 10884684]

Cui G, Meyer AC, Calin-Jageman I, Neef J, Haeseleer F, Moser T, Lee A 2007 $Ca^{2+}$-binding proteins tune $Ca^{2+}$-feedback to $Ca_V1.3$ channels in auditory hair cells. J. Physiol. 585, 791–803. [PubMed: 17947313]

Dulon D, Zajic G, Schacht J 1991 Differential motile response of isolated inner and outer hair cells to stimulation by potassium and calcium ions. Hear Res 52, 225–31. [PubMed: 2061210]

Gorny X, Mikhaylova M, Seeger C, Reddy PP, Reissner C, Schott BH, Helena Danielson U, Kreutz MR, Seidenbecher C 2012 AKAP79/150 interacts with the neuronal calcium-binding protein caldendrin. J Neurochem 122, 714–26. [PubMed: 22693956]

Haeseleer F, Sokal I, Verlinde CL, Erdjument-Bromage H, Tempst P, Pronin AN, Benovic JL, Fariss RN, Palczewski K 2000 Five members of a novel Ca2+-binding protein (CABP) subfamily with similarity to calmodulin. J. Biol. Chem. 275, 1247–1260. [PubMed: 10625670]

Hall JW 2007 New handbook of auditory evoked responses Pearson, Boston, MA.

Haynes LP, Tepikin AV, Burgoyne RD 2004 Calcium-binding protein 1 is an inhibitor of agonist-evoked, inositol 1,4,5-trisphosphate-mediated calcium signaling. J. Biol. Chem. 279, 547–555. [PubMed: 14570872]

Kasri NN, Holmes AM, Bultynck G, Parys JB, Bootman MD, Rietdorf K, Missiaen L, McDonald F, De Smedt H, Conway SJ, Holmes AB, Berridge MJ, Roderick HL 2004 Regulation of InsP3 receptor activity by neuronal $Ca^{2+}$-binding proteins. EMBO J. 23, 312–21. [PubMed: 14685260]

Kendall A, Schacht J 2014 Disparities in auditory physiology and pathology between C57BL/6J and C57BL/6N substrains. Hear Res 318, 18–22. [PubMed: 25456090]

Kim KY, Scholl ES, Liu X, Shepherd A, Haeseleer F, Lee A 2014 Localization and expression of CaBP1/caldendrin in the mouse brain. Neuroscience 268, 33–47. [PubMed: 24631676]

Koschak A, Reimer D, Huber I, Grabner M, Glossmann H, Engel J, Striessnig J 2001 a1D (Cav1.3) subunits can form L-type $Ca^{2+}$ channels activating at negative voltages. J. Biol. Chem. 276, 22100–22106.

Lee A, Westenbroek RE, Haeseleer F, Palczewski K, Scheuer T, Catterall WA 2002 Differential modulation of $Ca_V2.1$ channels by calmodulin and $Ca^{2+}$-binding protein 1. Nat. Neurosci. 5, 210–217. [PubMed: 11865310]

Liu WJ, Yang J 2015 Developmental expression of inositol 1, 4, 5-trisphosphate receptor in the post-natal rat cochlea. Eur J Histochem 59, 2486. [PubMed: 26150157]

Lv P, Sihn CR, Wang W, Shen H, Kim HJ, Rocha-Sanchez SM, Yamoah EN 2012 Posthearing $Ca^{2+}$ currents and their roles in shaping the different modes of firing of spiral ganglion neurons. J. Neurosci. 32, 16314–30.

Lv P, Kim HJ, Lee JH, Sihn CR, Fathabad Gharaie S, Mousavi-Nik A, Wang W, Wang HG, Gratton MA, Doyle KJ, Zhang XD, Chiamvimonvat N, Yamoah EN 2014 Genetic, cellular, and functional evidence for Ca2+ inflow through Cav1.2 and Cav1.3 channels in murine spiral ganglion neurons. J. Neurosci. 34, 7383–93. [PubMed: 24849370]

Meyer AC, Frank T, Khimich D, Hoch G, Riedel D, Chapochnikov NM, Yarin YM, Harke B, Hell SW, Egner A, Moser T 2009 Tuning of synapse number, structure and function in the cochlea. Nat Neurosci 12, 444–53. [PubMed: 19270686]

Michna M, Knirsch M, Hoda JC, Muenkner S, Langer P, Platzer J, Striessnig J, Engel J 2003 Cav1.3 (alpha1D) Ca2+ currents in neonatal outer hair cells of mice. J. Physiol. 553, 747–58. [PubMed: 14514878]

Mo ZL, Adamson CL, Davis RL 2002 Dendrotoxin-sensitive K(+) currents contribute to accommodation in murine spiral ganglion neurons. J. Physiol. 542, 763–78. [PubMed: 12154177]

Picher MM, Gehrt A, Meese S, Ivanovic A, Predoehl F, Jung S, Schrauwen I, Dragonetti AG, Colombo R, Van Camp G, Strenzke N, Moser T 2017 Ca2+-binding protein 2 inhibits Ca2+-channel inactivation in mouse inner hair cells. Proc. Natl. Acad. Sci. U. S. A. 114, E1717-E1726.

Platzer J, Engel J, Schrott-Fischer A, Stephan K, Bova S, Chen H, Zheng H, Striessnig J 2000 Congenital deafness and sinoatrial node dysfunction in mice lacking class D L-type $Ca^{2+}$ channels. Cell 102, 89–97. [PubMed: 10929716]

Schrauwen I, Helfmann S, Inagaki A, Predoehl F, Tabatabaiefar MA, Picher MM, Sommen M, Seco CZ, Oostrik J, Kremer H, Dheedene A, Claes C, Fransen E, Chaleshtori MH, Coucke P, Lee A, Moser T, Van Camp G 2012 A mutation in CABP2, expressed in cochlear hair cells, causes autosomal-recessive hearing impairment. Am J Hum Genet 91, 636–45. [PubMed: 22981119]

Simon MM, Greenaway S, White JK, Fuchs H, Gailus-Durner V, Wells S, Sorg T, Wong K, Bedu E, Cartwright EJ, Dacquin R, Djebali S, Estabel J, Graw J, Ingham NJ, Jackson IJ, Lengeling A, Mandillo S, Marvel J, Meziane H, Preitner F, Puk O, Roux M, Adams DJ, Atkins S, Ayadi A, Becker L, Blake A, Brooker D, Cater H, Champy MF, Combe R, Danecek P, di Fenza A, Gates H, Gerdin AK, Golini E, Hancock JM, Hans W, Holter SM, Hough T, Jurdic P, Keane TM, Morgan H, Muller W, Neff F, Nicholson G, Pasche B, Roberson LA, Rozman J, Sanderson M, Santos L, Selloum M, Shannon C, Southwell A, Tocchini-Valentini GP, Vancollie VE, Westerberg H, Wurst W, Zi M, Yalcin B, Ramirez-Solis R, Steel KP, Mallon AM, de Angelis MH, Herault Y, Brown SD 2013 A comparative phenotypic and genomic analysis of C57BL/6J and C57BL/6N mouse strains. Genome Biol 14, R82. [PubMed: 23902802]

Sinha R, Lee A, Rieke F, Haeseleer F 2016 Lack of CaBP1/Caldendrin or CaBP2 Leads to Altered Ganglion Cell Responses. eNeuro 3.

Tong B, Hornak AJ, Maison SF, Ohlemiller KK, Liberman MC, Simmons DD 2016 Oncomodulin, an EF-Hand Ca2+ Buffer, Is Critical for Maintaining Cochlear Function in Mice. J. Neurosci. 36, 1631–5. [PubMed: 26843644]

Weisz CJ, Lehar M, Hiel H, Glowatzki E, Fuchs PA 2012 Synaptic transfer from outer hair cells to type II afferent fibers in the rat cochlea. J. Neurosci. 32, 9528–36. [PubMed: 22787038]

Yang PS, Alseikhan BA, Hiel H, Grant L, Mori MX, Yang W, Fuchs PA, Yue DT 2006 Switching of $Ca^{2+}$-dependent inactivation of $Ca_V1.3$ channels by calcium binding proteins of auditory hair cells. J. Neurosci. 26, 10677–10689.

Yang T, Scholl ES, Pan N, Fritzsch B, Haeseleer F, Lee A 2016 Expression and Localization of CaBP Ca2+ Binding Proteins in the Mouse Cochlea. PLoS One 11, e0147495.

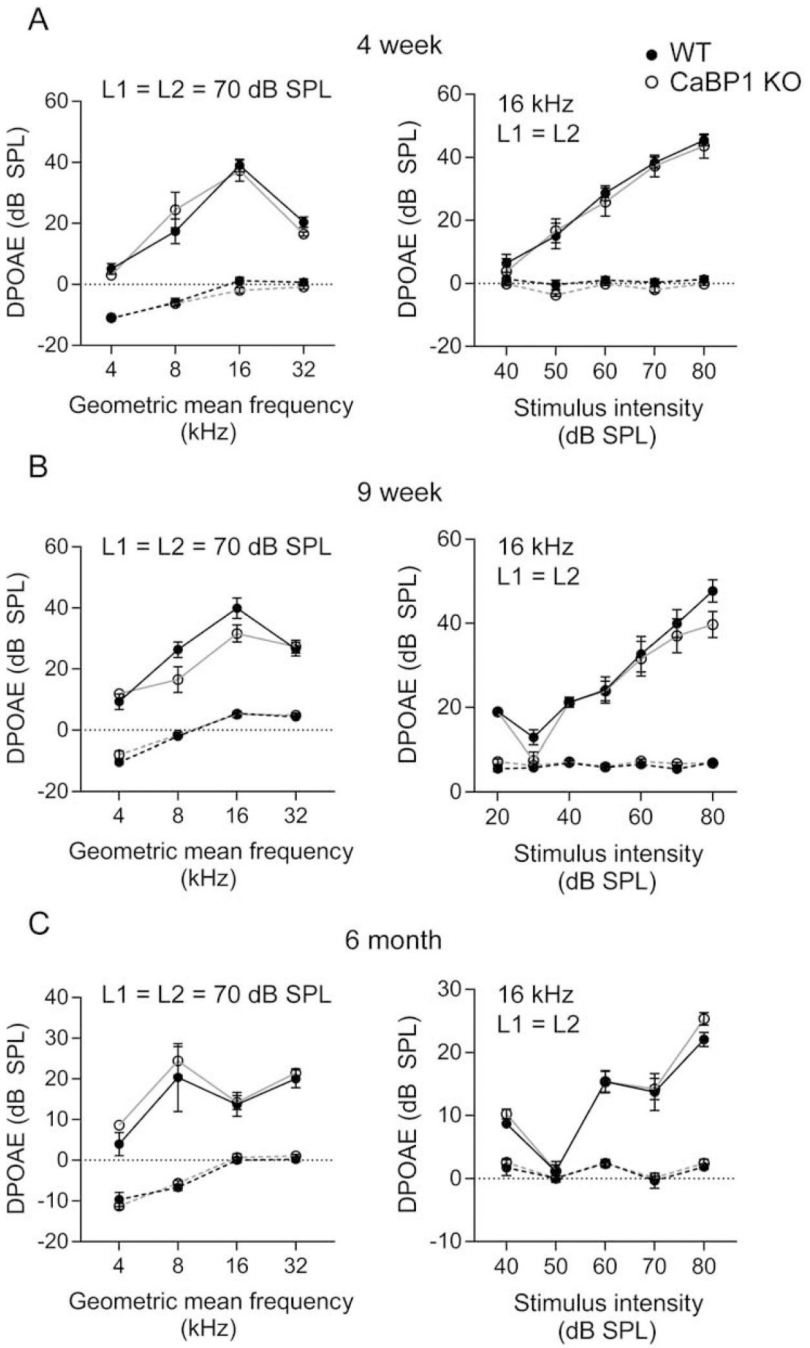


**Figure 1. DPOAEs are not affected in CaBP1 KO mice.**

DPOAEs were measured in 4-week-old (A), 9-week-old (B) and 6-month-old (C) mice. For each mouse, only the right ear was recorded. Points connected by dashed lines represent the noise floor, which was calculated by averaging the amplitude five points before and five points after frequency 2F2 - F1. *Left,* Mean 2F2-F1 DPOAE amplitudes ± SEM at F2/F1 = 1.2 plotted against the geometric mean of F1 and F2. The two tones (F2/F1=1.2) were applied at the same amplitude at 70 dB SPL. There was no significant difference between WT and CaBP1 KO mice ($F(1,56) < 0.01$, $p = 0.95$ for 4-week, n = 8 WT, 8 CaBP1 KO

mice; $F(1,48) = 3.60$, $p = 0.064$ for 9-week, n = 7 WT, 7 CaBP1 KO mice; $F(1,32) = 1.37$, $p = 0.25$ for 6-month, n = 4 WT, 6 CaBP1 KO mice, each by 2- way ANOVA). *Right*, mean DPOAE amplitudes ± SEM for F2 at 16 kHz was plotted against the stimulus intensity (L1 = L2). There was no significant difference between WT and CaBP1 KO mice ($F(1,70) = 0.396$, $p = 0.53$ for 4-week, $F(1,84) = 3.03$, $p = 0.09$ for 9-week, $F(1,40) = 1.19$, $p = 0.29$ for 6-month, each by 2- way ANOVA).

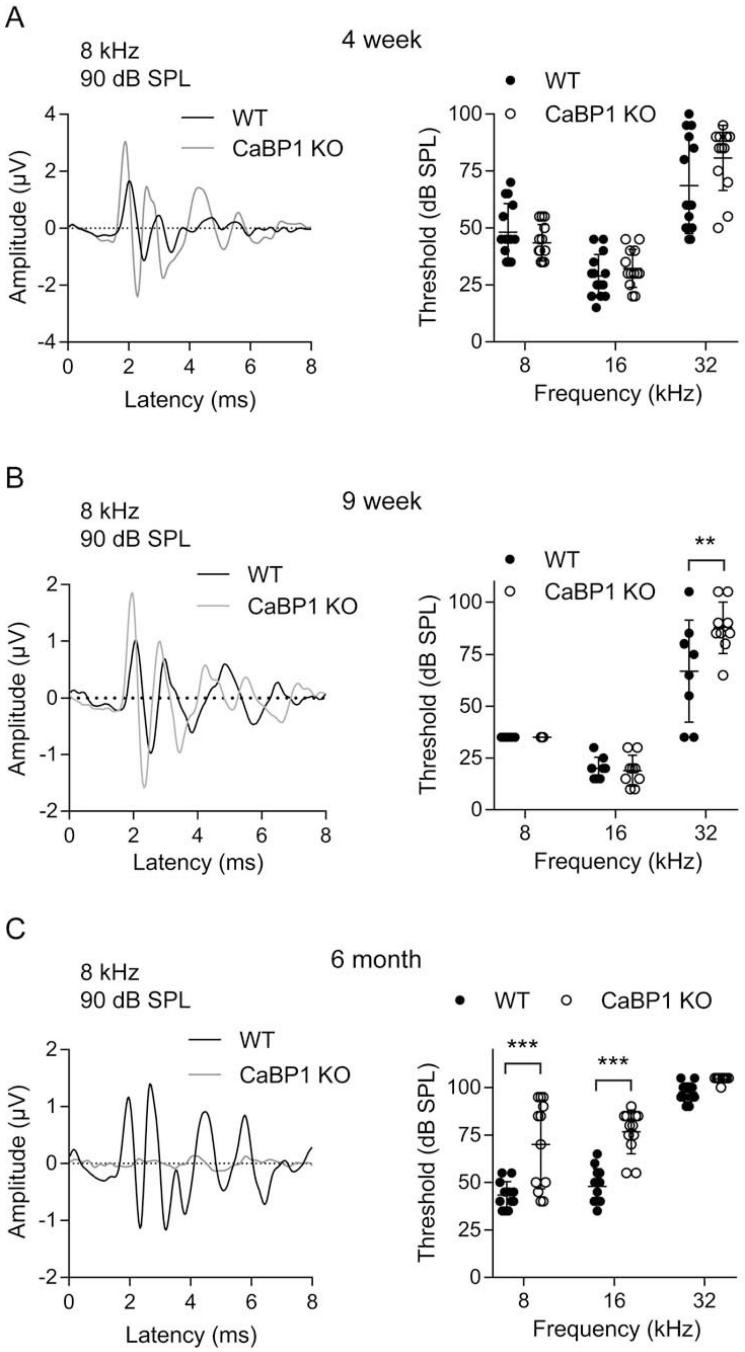


**Figure 2. ABR thresholds are increased with age in CaBP1 KO mice.**

ABRs were measured in 4-week (A), 9-week (B) and 6-month (C) old mice. *Left*, representative traces from ABRs using 8 kHz, 90 dB SPL stimulus. *Right,* ABR thresholds are plotted for 8-, 16-, and 32-kHz stimuli. Both left and right ears were measured separately. Each data point represents the average threshold from one mouse and bars represent mean ± SD. (A) *Left*, traces are from WT and CaBP1 KO mice with the same threshold (45 dB SPL). *Right,* There was no difference in ABR thresholds in 4-week old CaBP1 KO and WT mice at 8 kHz (44 ± 8 dB SPL for CaBP1 KO vs. 48 ± 12 dB SPL for

WT), 16 kHz (32 ± 8 dB SPL for CaBP1 KO vs. 29 ± 9 dBSPL for WT), or 32 kHz (81 ± 14 dB SPL for CaBP1 KO vs. 69 ± 21 dB SPL for WT). $F(1, 75) = 1.524$, $p = 0.221$, by 2-way ANOVA; n = 10 WT, 10 CaBP1 KO mice. (B) *Left*, Representative traces were from WT and CaBP1 KO mice with the same threshold (35 dB SPL). *Right*, By 9 weeks of age, the threshold was not different between genotypes at 8 kHz (35 ± 0 dB SPL for both) or 16 kHz (19 ± 7 dB SPL for CaBP1 KO vs. 20 ± 5 dB SPL for WT), but was significantly greater at 32 kHz in CaBP1 KO mice (88 ± 12 dB SPL) than in WT mice (67 ± 24 dB SPL). Interaction $F(2,45) = 4.852$, $p = 0.012$ by 2-way ANOVA; by post hoc Bonferroni's multiple comparisons test, $t(45) = 3.713$, $p = 0.002$ at 32 kHz; n = 8 WT, 9 CaBP1 KO mice). (C) *Left*, Representative traces were from mice with thresholds of 45 dB SPL for WT and 70 dB SPL for C-KO mice. *Right,* By 6 months, thresholds were elevated in CaBP1 KO mice at 8 kHz (70 ± 23 dB SPL for CaBP1 KO vs. 43 ± 7 dB SPL for WT) and at 16 kHz (77± 12 dB SPL for CaBP1 KO vs 48 ± 9 dB SPL for WT) but not at 32 kHz (105 ± 1 dB SPL for CaBP1 KO vs. 98 ± 5 dB SPL for WT). Interaction $F(2, 66) = 6.114$, $p = 0.004$ by 2-way ANOVA; by post hoc Bonferroni's multiple comparisons test, $t(66) = 5.516$, $p < 0.001$ for 8 kHz, $t(66) = 5.947$, $p < 0.001$ for 16 kHz; n = 12 WT, 12 CaBP1 KO mice).

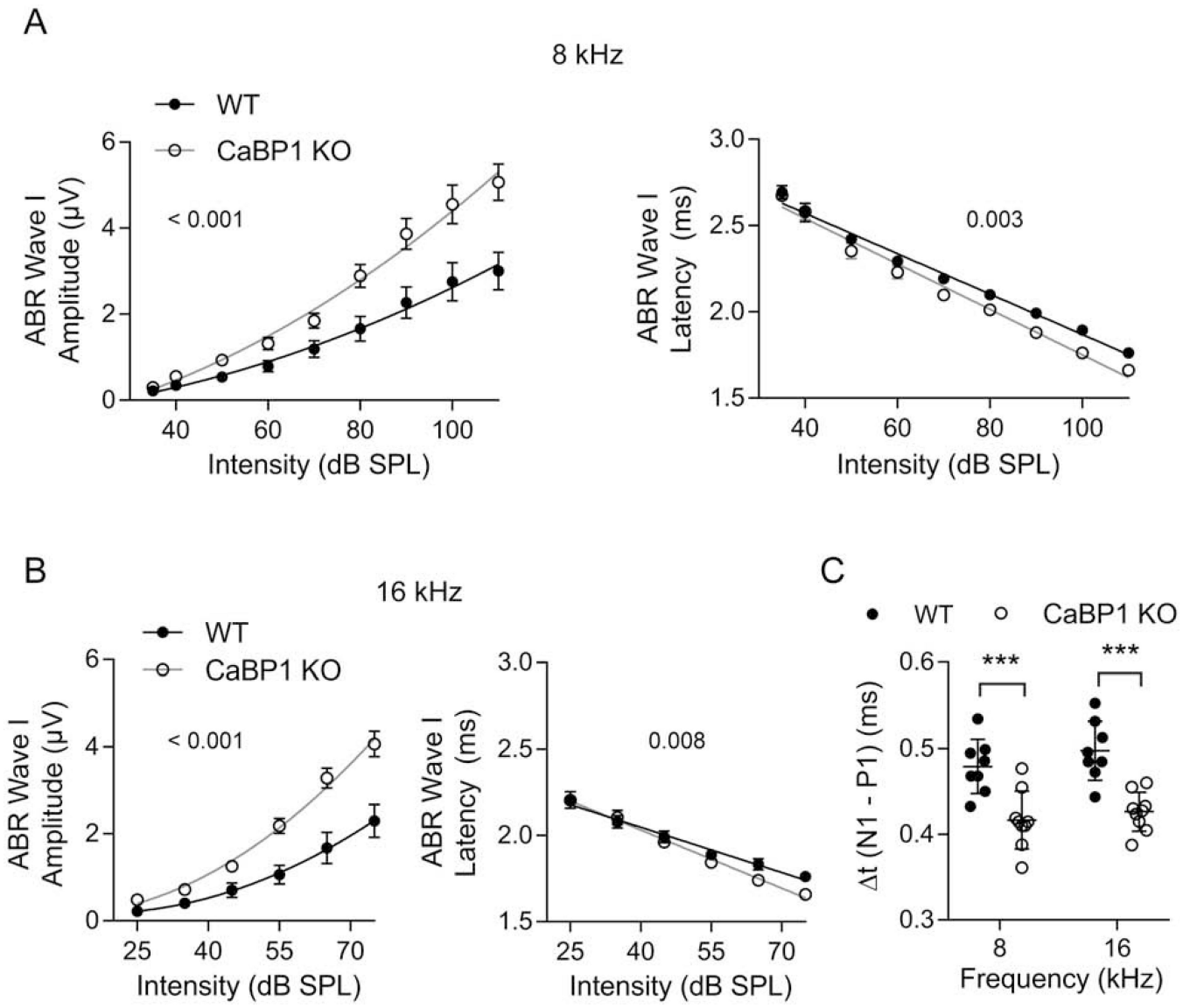


**Figure 3. Wave I amplitudes are increased and latencies are reduced in ABRs from 9-week old CaBP1 KO mice.**

(A-B) Wave I amplitude (*left*) and latency (*right*) from ABRs using 8 kHz (A) and 16 kHz (B) stimuli at the indicated dB SPL are plotted for WT and CaBP1 KO mice. Wave I amplitudes were significantly greater ($F(3,145) = 29.25$, $p < 0.001$ at 8 kHz; $F(3,105) = 31.35$, $p < 0.001$ at 16 kHz by extra sum of squares F-test) and latency was shorter ($F(1,15) = 12.41$, $p = 0.003$ for intercept at 8 kHz; $F(1,8) = 12.08$, $p = 0.008$ for slope at 16 kHz by analysis of covariance) in CaBP1 KO mice compared to WT mice. Points represent mean, error bars represent SEM. (C) The latency interval between P1 and N1 was significantly shorter in CaBP1 KO mice than in WT mice at 8 kHz (0.42 ± 0.03 ms for CaBP1 KO vs. 0.48 ± 0.03 ms for WT) and at 16 kHz (0.43 ± 0.02 ms for CaBP1 KO vs. 0.50 ± 0.03 ms for WT; $F(1,15) = 25.56$, $p < 0.001$, 2-way ANOVA; $t(30) = 4.163$, $p < 0.001$ for 8 kHz, $t(30) = 4.735$, $p < 0.001$ for 16 kHz by Bonferroni's post hoc test). Each point represents one mouse

and error bars represent SD. For each mouse (n = 8 WT, 9 CaBP1 KO mice), the average of responses recorded in left and right ears was used. ***, $p < 0.001$.

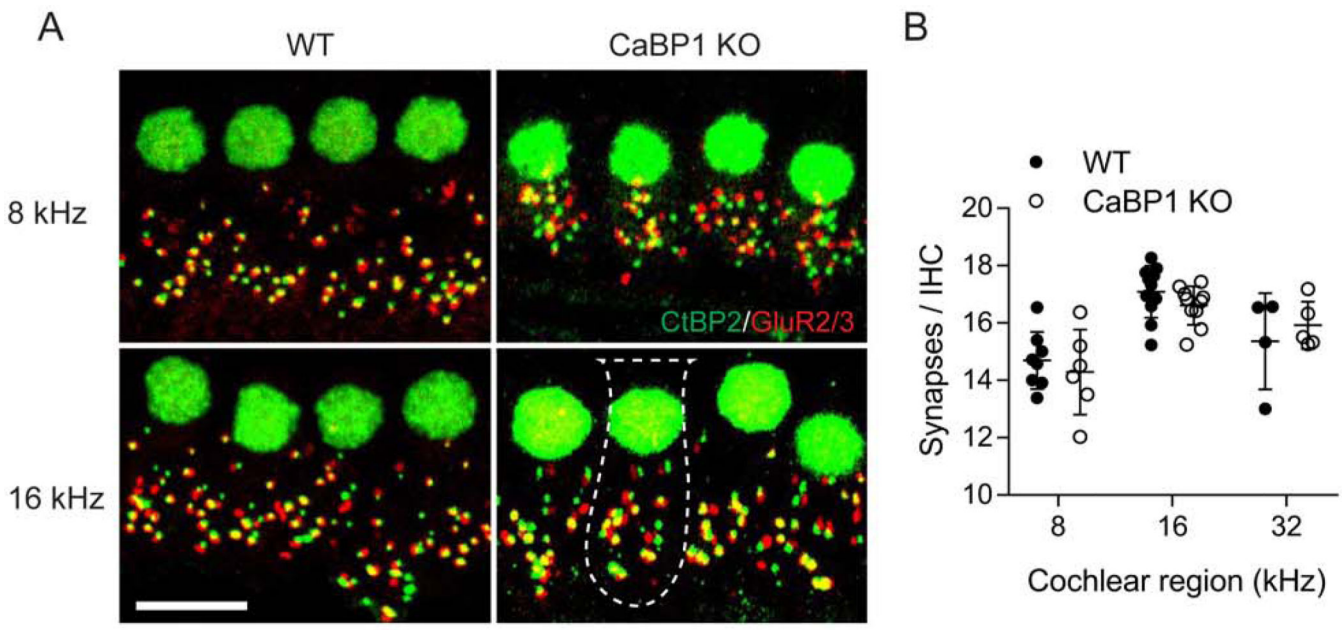


**Figure 4. The number of IHC synapses is not affected by loss of CaBP1.**

Cochleae from 9-week old WT and CaBP1 KO mice were double-labeled with antibodies against CtBP2 and GluR2/3 to label the pre-synaptic ribbons and IHC nuclei (green) and post-synaptic densities (red), respectively. Scale bar = 10 μm. (A) Maximal projections from representative confocal image stacks showing IHC synapses from WT and CaBP1 KO cochleae in regions corresponding to 8 kHz and 16 kHz frequencies. Dotted lines represent boundaries of IHC soma. (B) Quantification of the number of synapses per IHC. Synapses were defined as red and green puncta that were apposed to each other. The number of total synapses was divided by number of CtBP2-labeled nuclei and plotted for cochlear regions corresponding to the indicated frequencies. For each frequency region, synapses associated with 10–20 IHCs were counted (30–60/ cochlea). Points represents synapses/IHC per sample (from n = 8 WT and n = 8 CaBP1 KO mice); error bars represent SD. By 2-way ANOVA, there were no significant differences between synapses/IHC in WT and CaBP1 KO mice at 8 kHz (14 ± 1 for CaBP1 KO vs. 15 ± 1 for WT), 16 kHz (17 ± 1 for CaBP1 KO vs. 17 ± 1 for WT), or 32 kHz (16 ± 1 for CaBP1 KO vs. 15 ± 2 for WT). By 2-way ANOVA, there was a significant effect of frequency on the number of synapses/IHC ($F(2,38) = 21.51$; $p < 0.0001$) but no effect of genotype ($F(1,38) = 0.10$; $p = 0.75$) .

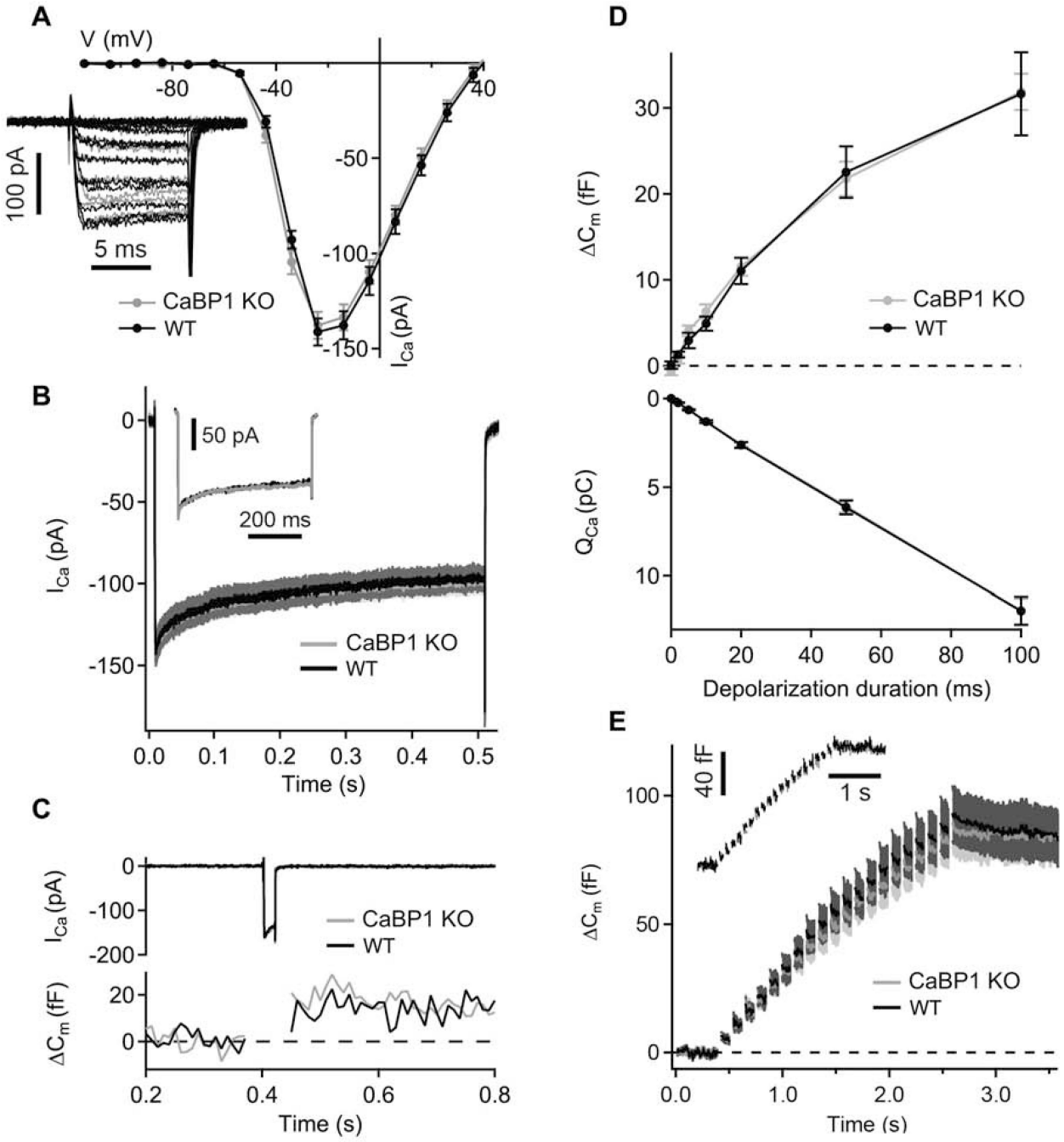


**Figure 5. Whole-cell $Ca^{2+}$ currents and exocytosis are not affected in CaBP1 KO IHCs.**

(A) Current-voltage relationship of $I_{Ca}$ in IHCs of CaBP1 KO and age-matched WT control mice (P17–22). Inset, representative traces corresponding to $I_{Ca}$ in WT (black) and CaBP1 KO (grey) IHCs. (B) Averaged and representative (inset) $I_{Ca}$ in response to 500-ms long depolarizations to −14 mV in CaBP1 KO (grey) and WT (black) IHCs are largely overlapping. (C) Representative $I_{Ca}$ (top) and membrane capacitance ($\Delta C_m$ ) responses (bottom) evoked by 20-ms depolarization to voltage evoking peak $I_{Ca}$. (D) Exocytosis ($\Delta C_m$; top) and the charge integral of $I_{Ca}$ ($Q_{Ca}$; bottom) upon depolarizations of different durations.

There was no significant difference in data from WT and CaBP1 KO IHCs ($p > 0.05$; Student's t test and Wilcoxon rank-sum test). (E) $\Delta C_m$ observed upon a train of 10-ms depolarizations (20 depolarizations with the interstimulus interval of 104 ms). Inset, representative $\Delta C_m$ response in WT (black) and CaBP1 KO (grey) IHCs. All responses are given as grand averages calculated from the means of the individual cells ± SEM. *A-B*, n = 9 WT and 17 CaBP1 KO cells; *D,* n = 8 WT and 17 CaBP1 KO cells; *E*, n = 8 WT and 16 CaBP1 KO cells.

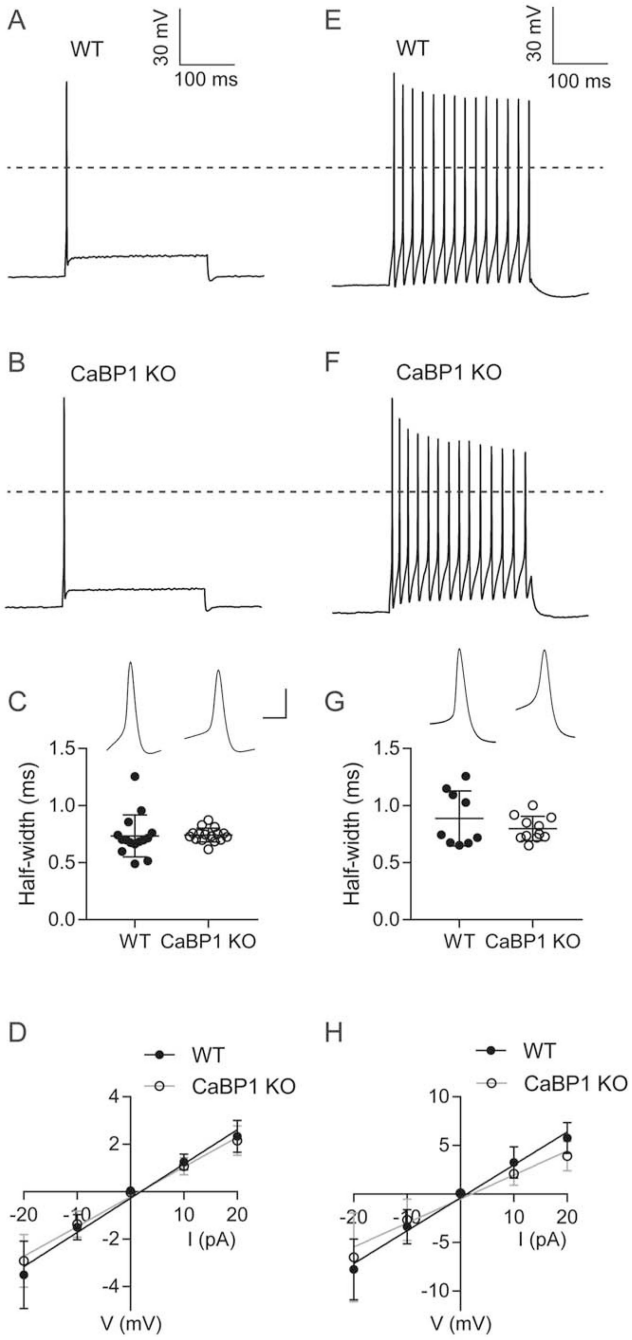


**Figure 6. APs and input resistance are altered in CaBP1 KO SGNs.**

Current clamp recordings were performed on SGNs from cultures obtained from P16–23 WT or CABP1 KO mice (11 cultures from different litters per genotype). Results are shown for rapidly adapting (A-D) and slowly adapting (E-H) SGNs. (A,B,E,F) Representative traces for APs elicited with a 250-ms, 0.1 nA current step. To identify AP thresholds, cells were held at −65 mV and current was injected to evoke 2-mV increments in membrane voltage for 250 ms. Dashed lines indicate 0 mV. (C,G) Half-width of the AP evoked by threshold current injection. Insets show representative APs. Scale bars, 60 mV (vertical), 4

ms (horizontal). There was no significant difference in the AP half-width in rapidly adapting SGNs (0.63 ± 5 ms for WT and 0.65 ± 0.05 ms for CaBP1 KO, t(29) = 0.70; $p = 0.50$ by unpaired t-test) or in slowly adapting SGNs (0.67 ± 0.06 ms for WT and 0.70 ± 0.05 ms for CaBP1 KO, t(18) = 1.2; $p = 0.24$ by unpaired t-test). Points represent measurements from different cells and bars represent mean ± SD. To test for variance, $p$-value was determined from $F$ test in $C$ ($F = 4.678$, $p < 0.01$) and Brown-Forsythe test using trimmed mean in $G$ ($F = 21.415$, $p = 0.020$). (D,H) Current-voltage plots. Graphs represent voltage responses from current injected in 10 pA increments for 1 s from rapidly adapting (D) and slowly adapting (H) neurons. Points represent mean ± SEM for WT (n = 16 neurons in D, n = 8 neurons in H) or CaBP1 KO (n = 18 neurons in D, n = 10 neurons in H). Input resistance was calculated as the slope of the linear fit for each neuron. Compared to WT, there was a significant decrease in the input resistance in CaBP1 KO SGNs for both rapidly adapting (126 ± 5 MΩ for CaBP1 KO vs. 144 ± 6 MΩ for WT; $F(1,166) = 5.70$, $p = 0.02$ by ANCOVA) and slowly adapting neurons (248 ± 22 for CaBP1 KO vs. 339 ± 23 for WT; $F(1,79) = 7.799$, $p < 0.01$, by ANCOVA).

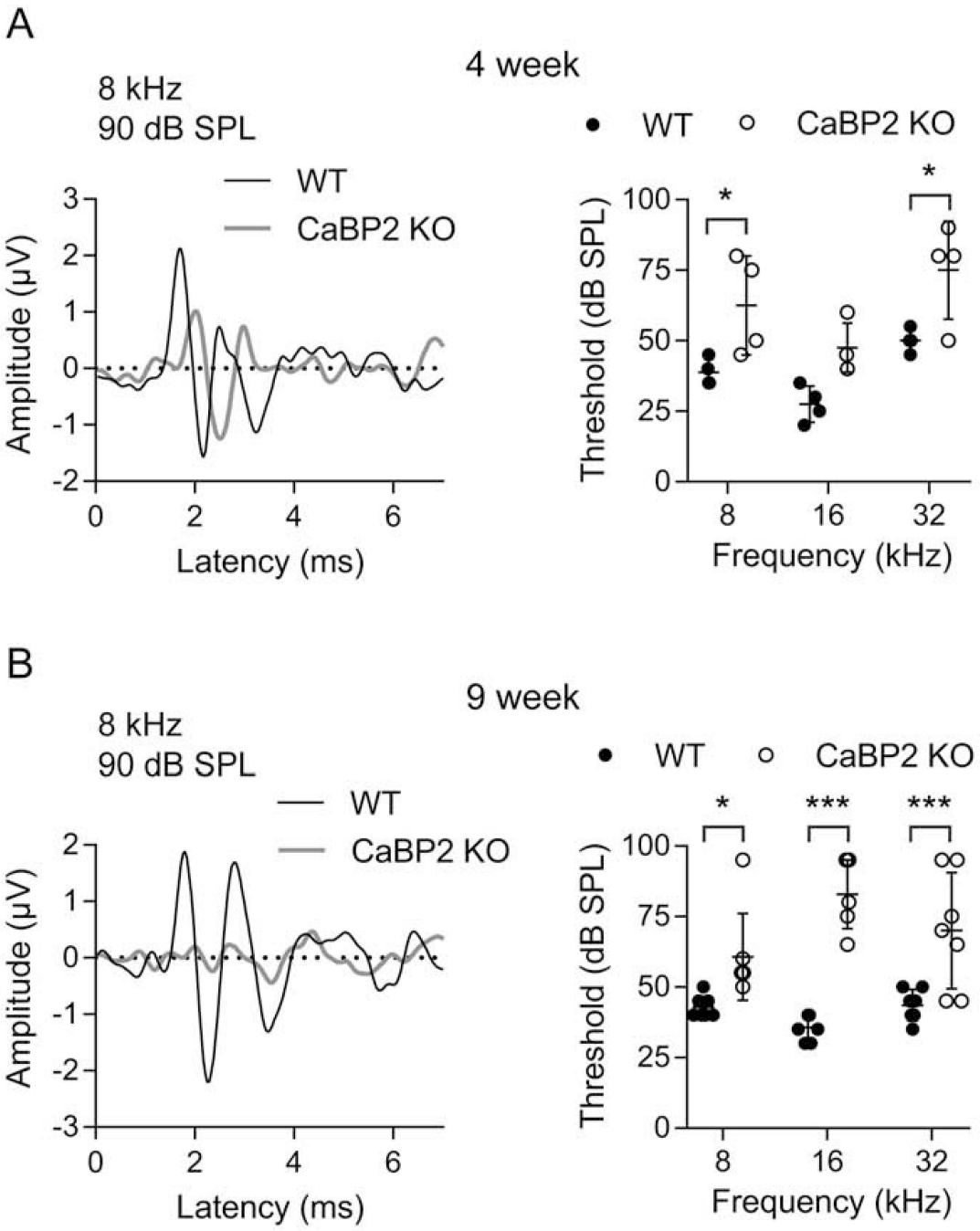


**Figure 7. ABR thresholds are increased in CaBP2 KO mice.**

ABRs were measured in 4-week-old (A) or 9-week-old (B) mice. Left panels, representative ABR waveforms for 4-week old or 9-week old WT and CaBP2 KO in response to 8 kHz, 90 dB SPL stimulus. Right panels, ABR thresholds plotted against stimulus frequency. Each data point represents result from one mouse and bars represent mean ± SD. For each mouse, the average of responses recorded in left and right ears was used. (A) At 4 weeks, there was a significant elevation in threshold in CaBP1 KO mice at 8 kHz ($F(1,18) = 24.73$, $p < 0.001$ for interaction by 2-way ANOVA. By post hoc Bonferroni's multiple comparisons test, $t(18)$

= 2.98, $p = 0.02$ for 8 kHz, and $t(18) = 3.13$, $p = 0.02$ for 32 kHz; n = 4 WT, 4 CaBP2 KO mice. (B) By 9 weeks, there was a significant increase in threshold of CaBP2 KO compared to WT mice at 8 kHz (61 ± 15 dB SPL for CaBP1 KO vs 43 ± 4 dB SPL for WT), 16 kHz (83 ± 12 dB SPL for CaBP1 KO vs. 37 ± 5 dB SPL for WT), and 32 kHz (70 ± 21 dB SPL for CaBP1 KO vs. 44 ± 6 dB SPL for WT). $F(2,36) = 5.426$, $p = 0.009$ for interaction by 2-way ANOVA. By post hoc Bonferroni's multiple comparisons test, $t(36) = 2.763$, $p = 0.03$ for 8 kHz, $t(36) = 7.293$, $p < 0.001$ for 16 kHz, $t(36) = 4.089$, $p < 0.001$ for 32 kHz; n = 7 WT, 7 CaBP2 KO mice.

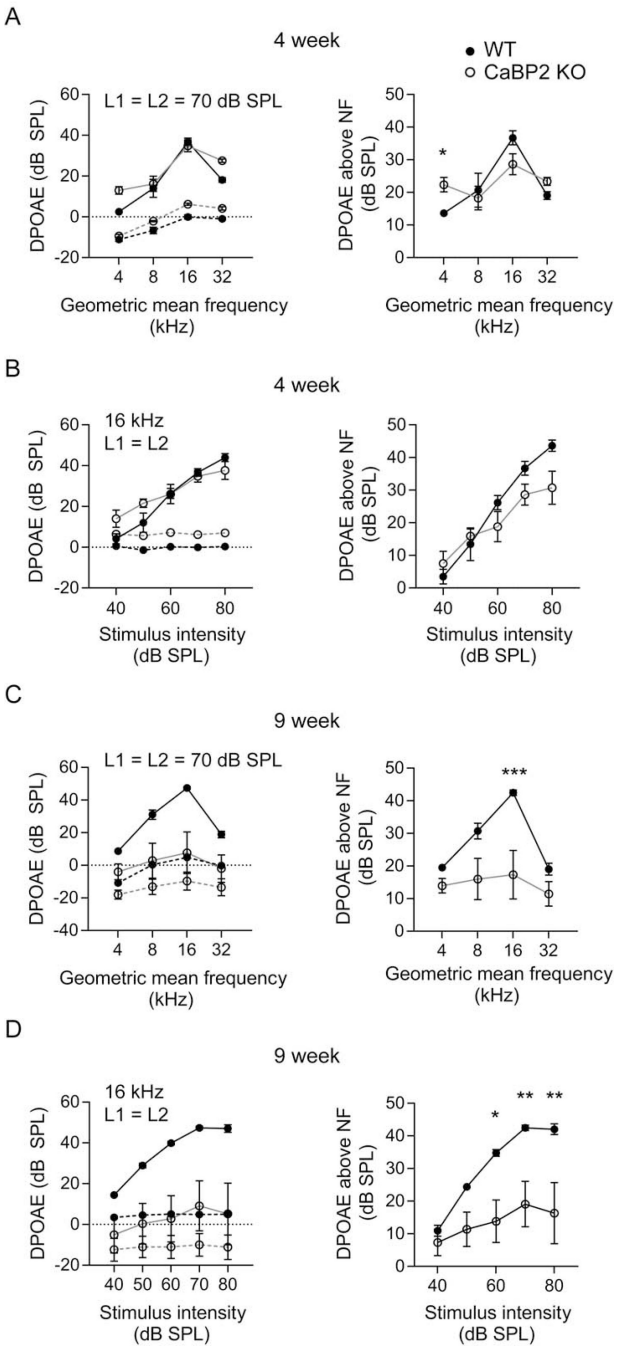


**Figure 8. DPOAE amplitudes are reduced in CaBP2 KO mice.**

DPOAEs were measured in 4-week-old (A-B) and 9-week-old (C-D) mice and noise floor was calculated as in Fig.2. *Left panels,* mean DPOAE s were plotted against geometric mean of F1 and F2 (A,C) or intensity (B,D). Points connected by dashed line represents noise floor. *Right panels,* the difference between the amplitude of noise floor and mean DPOAE amplitude is plotted against geometric mean of F1 and F2 (A,C) or intensity (B,D). (A) At 4 weeks, there was no difference between the DPOAEs of WT and CaBP2 KO (n = 6 mice each) plotted against frequency ($F(1,36) = 0.10$; $p = 0.76$ by 2-way ANOVA) or against

intensity ($F(1,45) = 4.19$, $p = 0.05$). By 9 weeks, DPOAE amplitudes were significantly depressed in CaBP2 KO mice compared to WT mice (n = 7 mice each) when plotted against frequency ($F(1,52) = 19.98$, $p < 0.001$ for genotype by 2-way ANOVA; by post-hoc Bonferroni's test, $t(52) = 4.241$, $p < 0.001$ for amplitude at 16 kHz) or intensity ($F(1,65) = 28.58$, $p < 0.001$ for genotype by 2-way ANOVA; by post-hoc Bonferroni's test, $t(65) = 2.889$, $p = 0.026$ for 60 dB, $t(65) = 3.223$, $p = 0.010$ for 70 dB, $t(65) = 3.548$, $p = 0.004$ for 80 dB. The statistical analysis was reported for DPOAEs above the noise floor (right panels). Points represent mean ± SEM.

**Table 1.**

Comparison of membrane properties of WT and C-KO SGNs.

| | Fast-adapting | | | | Slow-adapting | | | |
|---|---|---|---|---|---|---|---|---|
| | **Latency (ms)** | **RMP (mV)** | **Threshold (mV)** | **Height (mV)** | **Latency (ms)** | **RMP (mV)** | **Threshold (mV)** | **Height (mV)** |
| WT | 4.61 ± 0.42 | −59.44 ± 0.77 | −40.82 ± 0.76 | 63.48 ± 1.25 | 19.09 ± 3.03 | −54.11 ± 1.93 | −45.31 ± 2.68 | 67.32 ± 2.07 |
| C-KO | 5.13 ± 0.42 | −58.56 ± 0.97 | −40.04 ± 1.00 | 64.76 ± 1.34 | 19.55 ± 2.80 | −51.25 ± 1.97 | −44.14 ± 0.89 | 70.28 ± 1.42 |
| Statistics | $U = 115.5$, $p = 0.333$ | $t(32) = 0.698$, $p = 0.490$ | $t(32) = 0.607$, $p = 0.548$ | $t(32) = 0.696$, $p = 0.492$ | $t(17) = 0.112$, $p = 0.912$ | $t(19) = 1.105$, $p = 0.323$ | $^{*}t(9.78) = 0.415$, $p = 0.687$ | $t(18) = 1.207$, $p = 0.243$ |

Data are presented as mean ± SEM. For fast adapting SGNs: n = 16 WT and 18 C-KO cells. For slow-adapting SGNs: n = 8 WT and 11 C-KO cells. Unpaired *t* test was performed for normally distributed data. Otherwise, Mann Whitney test was performed and U value was reported.

*, Welch's t test was performed.